NANO LETTERS

pubs.acs.org/NanoLett Letter

Electron−Phonon Coupling in a Magic-Angle Twisted-Bilayer Graphene Device from Gate-Dependent Raman Spectroscopy and Atomistic Modeling

Andreij C. Gadelha,[#] Viet-Hung Nguyen,[#] Eliel G. S. Neto, Fabiano Santana, Markus B. Raschke, Michael Lamparski, Vincent Meunier, Jean-Christophe Charlier,[*] and Ado Jorio[*]

Cite This: *Nano Lett.* 2022, 22, 6069−6074 Read Online

ACCESS | Metrics & More | Article Recommendations | Supporting Information

ABSTRACT: The importance of phonons in the strong correlation phenomena observed in twisted-bilayer graphene (TBG) at the so-called magic-angle is under debate. Here we apply gate-dependent micro-Raman spectroscopy to monitor the G band line width in TBG devices of twist angles $\theta = 0°$ (Bernal), ∼1.1° (magic-angle), and ∼7° (large-angle). The results show a broad and p-/n-asymmetric doping behavior at the magic angle, in clear contrast to the behavior observed in twist angles above and below this point. Atomistic modeling reproduces the experimental observations in close connection with the joint density of electronic states in the electron−phonon scattering process, revealing how the unique electronic structure of magic-angle TBGs influences the electron−phonon coupling and, consequently, the G band line width. Overall, the value of the G band line width in magic-angle TBG is larger when compared to that of the other samples, in qualitative agreement with our calculations.

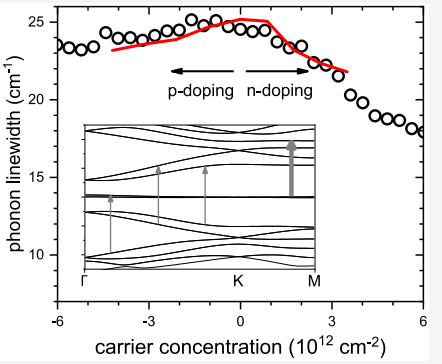

KEYWORDS: *graphene, Raman spectroscopy, atomistic modeling, electron−phonon interaction*

The unusual electronic structure of graphene, with massless Dirac Fermions, along with the relatively light C atoms bound together by strong covalent σ-bonds, is responsible for electron−phonon scattering that rules the lifetime of phonons, in departure from the broadly adopted adiabatic Born−Oppenheimer approximation.[1] The breakdown of the adiabatic Born−Oppenheimer approximation generates a Kohn anomaly,[2] which has been studied in graphite,[3] single-layer graphene,[1−4] double-layer graphene with the graphite-like AB (Bernal) stacking,[5−8] and in metallic carbon nanotubes[9−11] using Raman spectroscopy.[12] Electrons dress the phonon quasi-particles and thus modify phonon frequencies, decrease their lifetimes, and, ultimately, cause corresponding spectral broadening.[4] These effects in the Raman spectra were shown to be dependent on the materials Fermi level (E_F), because the electron−phonon coupling can be changed, including the suppression of some Raman scattering paths due to the Pauli exclusion principle, thereby offering a unique way to accurately monitor E_F in the family of sp^2 carbon nanostructures,[13] including the influence of different environments, such as different substrates.[14−16] Although phonon−phonon interactions also influence phonon properties,[3,17] within a low doping regime where the Fermi level changes are in the order of the phonon energies or smaller, the anharmonicities are negligible when compared to Kohn anomaly effects.[2]

Twisted-bilayer graphene (TBG) represents a new class of sp^2 carbon nanostructures for the development of graphene-based twistronics with novel properties, such as twist-angle θ-dependent van Hove singularities in the electronic density of states (DOS) for large-angle TBGs ($2° < \theta < 30°$);[18,19] unusual superconductivity at the magic-angle ($\theta \sim 1.1°$);[20] and lattice reconstruction with the formation of strain soliton and topological points for low-angle TBGs ($\theta < 1°$).[21−23] Recent spectroscopic and imaging resolved with nanometer spatial resolution (nano-Raman) measurements show that in the low-angle regime the electronic and phononic structures feature significantly localized properties.[23] Consequently, the C−C stretching energy uncertainty, as measured by the Raman G-band phonon line width (Γ_G), varies spatially, following the moiré lattice structure governed by atomic reconstruction. Additionally, it was shown, at the micrometric scale, that Γ_G reaches a maximum at the magic angle, decreasing toward the expected graphene line width far below and above 1°, both in the large- and low-angle domains. These findings motivate exploring the Kohn anomaly in TBGs using Raman spectroscopy gate-doping experiments. These experiments enable the quantification of the importance of electron−phonon in Γ_G, as

Received: March 4, 2022
Revised: July 21, 2022
Published: July 25, 2022

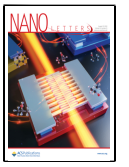

https://doi.org/10.1021/acs.nanolett.2c00905
Nano Lett. 2022, 22, 6069−6074

contrasted to other possible structural effects,[24−28] thus shedding light into the role of phonons in TBG strongly correlated phenomena.[29−36]

Figure 1a shows a simplified schematic of the electrochemical TBG devices. Electrochemical devices were utilized

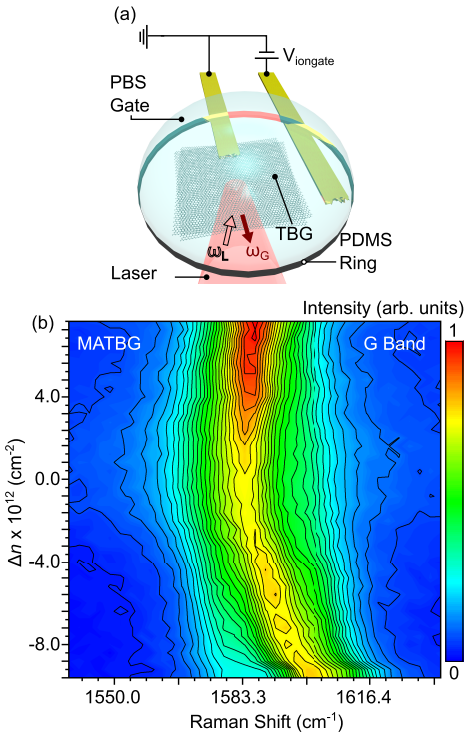

Figure 1. (a) Simplified schematics of the TBG electrochemical device with bottom illumination and Raman detection. We show the contacts (yellow stripes) with the electrical wiring, and the ionic liquid drop (transparent blue) covering the entire device. (b) magic-angle TBG G band spectra vs carrier concentration Δn.

because one can obtain higher doping capacities to tune the Fermi level, which is important to observe the results described here. Electrical contacts were prepatterned on a coverslip by optical lithography, followed by deposition of a 1 nm chromium adhesive layer and a 50 nm gold layer. TBG samples were prepared by a dry "tear-and-stack" method, using a polydimethylsiloxane (PDMS) semipyramidal stamp covered with a polycarbonate (PC) sheet, as described in ref 37. The TBGs were then transferred onto the prepatterned electrical contacts for *in situ* electrical and optical studies. An electrochemical gate composed of a phosphate-buffered saline (PBS) solution is utilized (NaCl, 0.137 M; KCl, 0.0027 M; Na_2HPO_4, 0.01 M; and KH_2PO_4, 0.0018 M). A potential ($V_{iongate}$) is applied to a free electrode that is not connected electrically to graphene, with $V_{iongate}$ kept low enough to avoid electrical breakdown, while the electrical contacts connected to graphene are grounded. The device was built directly on the coverslip, based on our experiences with twisted bilayers, which have shown to have less twist-angle disorder than samples built on hBN.[23,28,37,38] The ionic liquid behavior is calibrated utilizing a Bernal bilayer graphene deposited on 285 nm thick SiO_2, which has a known capacitance.[39] More details about the device structure and on how the carrier concentrations are determined can be found in the Supporting Information.

Micro-Raman scattering experiments were carried out on an inverted microscope, with a high N.A. = 1.4 oil-immersion objective, excited with a HeNe laser (λ = 633 nm), achieving ~400 nm spatial resolution. The backscattered light is collected by an spectrometer equipped with a charge-coupled device (CCD) and a 600 g/L grating (Andor Solis). Figure 1b shows the spectral evolution of the magic-angle TBG Raman G band spectra as a function of the carrier concentration (Δn), where positive and negative Δn were adopted for n- and p-doping, respectively. Spectra were obtained with 3 accumulations of 20 s (for Bernal and large-angle TBGs, 3 × 10 s of accumulation). We use laser powers lower than 1 mW in the sample to avoid laser-induced sample heating.

We fit the G bands with a single Lorentzian to extract their characteristics, including the band line widths (full width at half-maximum, fwhm, Γ_G) values, reported here after correction to account for the spectrometer resolution. By carrying out Raman mapping, we estimate contributions from inhomogeneity to the experimental Γ_G data to be smaller than 3 cm^{-1} (see refs 24, 26, and 40 and the Supporting Information for further details, including the 2D peak,[12] also named G′ in the literature, which is not addressed here, and the D-peak range showing the absence of defects in the sample).

The phonon frequency is given by $\omega_q^\nu = \omega_q^{(0)\nu} + \omega_q^{(2)\nu}$, where $\omega_q^{(0)\nu}$ and $\omega_q^{(2)\nu}$ are, respectively, the unperturbed phonon frequency and the frequency correction due to renormalization by the electron−phonon interaction (Kohn anomaly).[4,41] Although gate experiments change the intensities, frequencies, and line widths of different Raman bands in graphene-related systems,[4] here we focus on the G-band line width Γ_G behavior to collect information related to the electron−phonon coupling.

The phonon line width is directly obtained from the imaginary part of $\omega_q^{(2)\nu}$:

$$\Gamma_q^{\mathrm{ph},\nu} = \Im(\omega_q^{(2)\nu}) = 4\pi \sum_{n,m} \int \frac{dk}{A_{BZ}} |M_{ep}^{\nu}(k, k+q)|^2 \times [f(E_k^n) - f(E_{k+q}^m)]\, \delta(\hbar\omega_q^{(0)\nu} - E_{k+q}^m + E_k^n) \quad (1)$$

where E_k^n and E_{k+q}^m are the energies for the electronic states before and after the q-phonon mediated scattering, $f(E_k^n)$ is the Fermi distribution, $M_{ep}^{\nu}(k, k+q)$ is the electron−phonon matrix element, and A_{BZ} is the area of the first Brillouin zone where the k-integral is carried out. Throughout this work, theoretical results are calculated/presented within the moiré Brillouin zone.

Generally, previous work on sp^2 carbon systems[1−3,5−11,13] considered $M_{ep}^{\nu}(k, k+q)$ as weakly varying (almost constant over the experimental range), and the phonon behavior (frequency and line width) can be reduced to the calculation of the JDOS, while taking the Pauli exclusion principle into account: $\Gamma_G^{ph} \propto \mathrm{JDOS}\,(\hbar\omega_G)[f(-\hbar\omega_G/2) - f(\hbar\omega_G/2)]$, where ω_G is the frequency of G band phonons. This simplified expression reproduces the behavior of single-layer, AB-bilayer, and large-angle TBG, but it fails when applied to magic-angle TBG, as shown in this work. In the former cases, the simple electronic structures, with linear or parabolic energy dispersions, are obtained in a large range of energies around the E_F; therefore, their low-energy bands can be accurately modeled using a single-particle tight-binding model, even when the system is doped. However, around and below the magic-

https://doi.org/10.1021/acs.nanolett.2c00905
Nano Lett. 2022, 22, 6069−6074

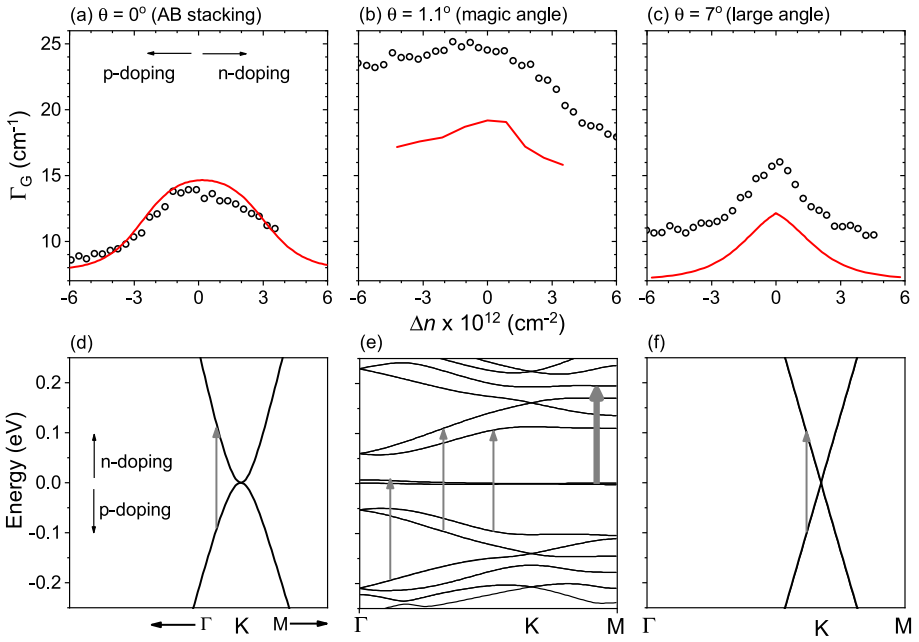

Figure 2. (a–c) Gate-dependent G-band fwhm, Γ_G, and (d–f) electronic band structures for Bernal (a, d, $\theta = 0°$), magic-angle (b, e, ∼1.1°), and large angle (c, f, ∼7°) TBGs, near the Fermi level (0 eV). (a–c) The dots are experimental data, while red lines are theoretical predictions upshifted by $\Delta_G^{(0)} = 7$ cm^{-1} to fit the $\theta = 0°$ AB-stacked data. (d–f) The gray arrows indicate the electronic transitions induced by the G band (∼0.2 eV) phonon interaction. (e) The thick arrow represents a large JDOS near the flat bands.

angle TBGs, strong electron localization occurs near E_F,[42] therefore leading to strong Coulomb interactions.[43] These Coulomb interactions have been shown to smooth out the spatial distribution of charge carriers and to lead to significant changes in the electronic structure upon doping.[44−49] Due to these doping effects on the electronic structure and the effects of atomic reconstruction on phonon properties in small-angle TBG,[27] the doping dependence of electron−phonon interactions in magic-angle TBG cannot be described simply as in the cases of nontwisted systems and large angle TBG, as detailed below.

In order to take into account the doping effects, we first use an adjusted electronic model, i.e., a single-particle tight-binding Hamiltonian modified by adding a Hartree potential term,[46,47] that depends on doping concentration (see the Supporting Information). We then perform atomistic calculations (11164 atoms in the magic-angle TBG unit cell) of the frequency $\omega_q^{(2)\nu}$ in eq 1, with the electron−phonon matrix elements for the G band defined as[32,50]

$$M_{ep}^{G}(k, n, m) = \sqrt{\frac{\hbar}{2M_C\omega_G^0}} \sum_{i\alpha} e_{i\alpha}^{G} \langle m, k|\partial_{i\alpha}\hat{H}|n, k\rangle \quad (2)$$

where M_C is the mass of a carbon atom, $\partial_{i\alpha}\hat{H}$ is the derivative of the tight-binding Hamiltonian with respect to the position of the ith atom along the α-axis, $|n, k\rangle$ are the eigenfunctions of $\hat{H}$ with eigenvalues E_k^n, and the polarization vectors $e_{\kappa\alpha}^{G}$ come from phonon calculations.[27]

The open bullets in Figure 2a−c display the experimental gate-dependent G-band fwhm (Γ_G) for: (a) AB (Bernal)-stacked bilayer graphene ($\theta = 0°$); (b) magic-angle TBG ($\theta \sim 1.1°$); and (c) large-angle TBG ($\theta \sim 7°$). Three aspects that summarize the findings are highlighted here: (i) Overall, the value for Γ_G is roughly 10 cm^{-1} larger for the magic-angle TBG (Figure 2b) as compared to the other samples (Figures 2a,c). (ii) The magic-angle sample exhibits an anomalously broad and p-/n-asymmetric doping dependence. (iii) The large angle TBG (Figure 2c) shows a kink in the Γ_G gate-dependence at the neutrality point, different from the other samples.

To explain the three observed aspects in the experimental data, the theoretical results obtained using eq 1 with the matrix elements from eq 2 are included in Figure 2 (red lines in panels a−c). The calculated results are all upshifted by $\Delta_G^{(0)} = 7$ cm^{-1} to fit the data for the Bernal bilayer graphene ($\theta = 0°$), consistent with values reported in the literature and attributed to nonelectron−phonon coupling effects (anharmonicity) and inhomogeneous broadening.[4,7,8] The red line for the magic-angle TBG in Figure 2b is limited to low doping values ($\Delta n \leq \pm 4 \times 10^{12}$ cm^{-2}) because the model utilized here is only valid when the doping is limited to the Fermi levels near the flat bands (see inadequate extended calculation in the Supporting Information).

Considering (i), the overall average value for Γ_G, the higher values obtained theoretically for the magic-angle sample (red line in Figure 2b) are due to the higher JDOS in the G-band electron−phonon coupling, as indicated by the gray arrows in Figure 2d−f (and further illustrated in the Supporting Information). Therefore, the JDOS analysis can explain roughly half (∼5 cm^{-1}) of the observed higher Γ_G in the magic-angle TBG, and our results are in qualitative agreement with refs. 32 and 36.

The experimental data for Γ_G in the large-angle TBG (bullets in Figure 2c) are roughly 3 cm^{-1} higher than the calculated results (red line), and the discrepancy here is related to the lower calculated JDOS for a linearly dispersed electronic sctucture (Figure 2f) as compared to the parabolic dispersion in the AB-stacked bilayer graphene (Figure 2d). Looking only at the experimental data, however, the Γ_G values for $\theta = 0°$ (Figure 2a) and $\theta = 7°$ (Figure 2c) TBGs are close to each other, while the higher values of Γ_G for magic-angle TBGs (Figure 2b) have been observed consistently in other doping-independent measurements.[23,40] We also note that the extrinsic

https://doi.org/10.1021/acs.nanolett.2c00905
Nano Lett. 2022, 22, 6069−6074

inhomogeneous broadening are expected to be present in all samples, and they have been estimated to be less than ∼3 cm^{-1} (see the Supporting Information).

Now we analyze the most striking result, that is, (ii) the considerably broader and asymmetric Γ_G-dependence on Δn for magic-angle TBG (Figure 2b), as compared to that for the AB bilayer (Figure 2a) and large-angle TBG (Figure 2c). The broader dependence on Δn is due to the flat band near the neutrality point in magic-angle TBGs (Figure 2e), which requires a considerable amount of carriers to be filled or emptied, associated with the presence of other electronic bands within the G band phonon energy range.

As for the asymmetric p/n results, the asymmetry is nicely explained by our atomistic simulations (see the red line in Figure 2b), where we include the smoothing of charge inhomogeneities due to strong Coulomb interactions in magic-angle TBG. The variation of Γ_G (as described in eq 1) when varying the doping concentration is dependent on both the electron−phonon matrix elements (eq 2) and the number of available electronic states mediating the G-phonon scatterings (i.e., JDOS at $\hbar\omega_G \sim 0.197-0.200$ eV). Therefore, the change in both these quantities explain the reduction of Γ_G when magic-angle TBG is doped. In magic-angle TBG, there are both strongly real-space electronic localization[42] in the undoped case and significant charge smoothening effects[45] when the system is doped, which can result in the significant change not only in JDOS but also in electronic wave functions (accordingly, M_{ep}^G) in eq 2 upon doping. This point is very different from Bernal and large-angle TBG systems, where M_{ep}^G is considered as weakly varying with the doping. As illustrated in Figure 3, these changes in the electronic structure lead to a reduction of available electronic states that mediate the G-phonon scatterings (see the gray arrows in Figure 3a−c), resulting in different JDOSs (Figures 3d−f and S2). These changes explain, first, the reduction of phonon line width when magic-angle TBG is doped and, second, why the phonon line width reduction is observed to be stronger in the n-doped regime than in the p-doped regime (see Figure 3), as experimentally observed (see Figure 2b).

Finally we explain (iii), the sharp peak (kink) observed at zero doping for large-angle TBG (see Figure 2c). The Γ_G dependence on the E_F in this case, as well as for Bernal stacking, can be approximately described by the function $f(-\hbar\omega_G/2) - f(-\hbar\omega_G/2)$ that smoothly varies with the E_F (including the region around $E_F = 0$). In the Bernal bilayer system, Δn scales as $\Delta n \propto E_F$ because of its parabolic low-energy bands. The large-angle TBGs, however, exhibit a Dirac-like linear energy dispersion, similar to that observed in monolayer graphene; therefore, $\Delta n \propto E_F^2$.[51] As a consequence, a kink at zero doping is observed for large-angle TBG. Note that the simple descriptions above are no longer valid in the case of magic-angle TBG, because its flat electronic bands and doping effects make the model significantly different (see the electronic band structures illustrated in Figure 2d−f).

In summary, micro-Raman spectroscopy is used to study the G band line width (Γ_G) in TBG devices of twist angles $\theta = 0°$ (Bernal), ∼1.1° (magic-angle), and ∼7° (large-angle), and atomistic modeling is carried out in order to explain the observations. The gate-dependent Γ_G exhibits a broad and p-/n-asymmetric Γ_G doping behavior at the magic angle, in clear contrast to the behavior observed for both larger and smaller twist angles. The results are rationalized by our calculations as due to the unusual electronic structure in the magic-angle

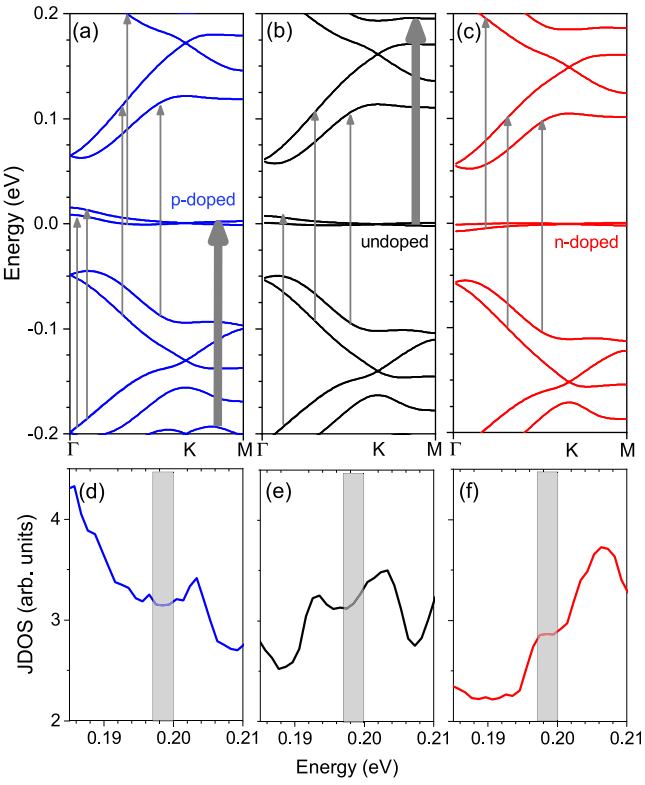

Figure 3. Doping effect on the electronic structure of magic-angle twisted bilayer graphene: (a, d) p-doped, (b, e) undoped [analogous to Figure 2e], and (c, f) n-doped. (a−c) Electronic band structures, with the Fermi level kept at 0 eV. Arrows are as explained in the caption to Figure 2. (d−f) JDOS. The gray stripe indicates the G-band energy range 0.197−0.200 eV.

TBG, specifically the flat bands near the Fermi level, and its consequences in the JDOS for the electron−phonon scattering. Furthermore, magic-angle TBGs always show larger Γ_G values, in agreement with (gate-independent) experimental results in the literature.[23,40] Our results are also in qualitative agreement with theoretical work in the literature that predicts stronger electron−phonon coupling in magic-angle TBG.[36] Although the results here are limited to the Raman-active in-plane optical phonon at Γ (G band), calculations in the literature indicate that the largest contribution to the total electron−phonon coupling strength λ comes from the in-plane optical phonon modes near $\omega_D = 167$ and $\omega_G = 197$ meV, with momenta corresponding to $q = K, K'$, and Γ, respectively. As established in the literature, together they contribute to about 70% of λ ($\lambda_D = 0.914$ and $\lambda_G = 0.648$).[36]

Nano-Raman spectroscopy showed larger Γ_G values localized at AA sites in reconstructed small-angle TBGs.[23] We speculate that an optimized situation happens for the magic angle, improving the electron−phonon coupling not only locally at the AA sites but also all over the sample. A nano-Raman spectrometer with very high spatial resolution (in the nanometer range or below) would be needed to demonstrate this assumption.

Our results support previous theoretical studies that investigated the relevance of electron−phonon coupling in magic-angle TBGs in order to accurately understand strongly correlated phenomena, such as superconductivity and its robustness in twisted layered systems.[32,36] It is important to stress, however, that the G band energy is too high as

https://doi.org/10.1021/acs.nanolett.2c00905
Nano Lett. 2022, 22, 6069−6074

compared to the typical bandwidth in magic-angle TBG, which reduces the direct importance of a G-band mediated process to superconductivity. The effective coupling to the G-band phonon can be, however, a proxy to the same enhancement to the lower energy acoustic branches.

■ ASSOCIATED CONTENT

Supporting Information

The Supporting Information is available free of charge at https://pubs.acs.org/doi/10.1021/acs.nanolett.2c00905.

Details about the theory, including structural relaxation and phonon calculations, the electronic models, the modeling of Phonon Kohn anomalies, and comment about the limited doping range calculations for magic-angle twisted-bilayer graphene; further experimental information, including details about the D, G, and 2D (or G′) band spectra and spectral fitting, device structure, and characterization (PDF)

■ AUTHOR INFORMATION

Corresponding Authors

Jean-Christophe Charlier − *Institute of Condensed Matter and Nanosciences, Université Catholique de Louvain (UCLouvain), Louvain-la-Neuve 1348, Belgium*; Email: jean-christophe.charlier@uclouvain.be

Ado Jorio − *Physics Department, Universidade Federal de Minas Gerais, Belo Horizonte, Minas Gerais 31270-901, Brazil*; orcid.org/0000-0002-5978-2735; Email: adojorio@fisica.ufmg.br

Authors

Andreij C. Gadelha − *Physics Department, Universidade Federal de Minas Gerais, Belo Horizonte, Minas Gerais 31270-901, Brazil; Department of Physics, and JILA, University of Colorado at Boulder, Boulder, Colorado 80309, United States*; orcid.org/0000-0002-6350-7680

Viet-Hung Nguyen − *Institute of Condensed Matter and Nanosciences, Université Catholique de Louvain (UCLouvain), Louvain-la-Neuve 1348, Belgium*; orcid.org/0000-0001-6729-3520

Eliel G. S. Neto − *Physics Institute, Universidade Federal da Bahia, Salvador, Bahia 40170-115, Brazil*; orcid.org/0000-0002-4658-3243

Fabiano Santana − *Physics Department, Universidade Federal de Minas Gerais, Belo Horizonte, Minas Gerais 31270-901, Brazil*; orcid.org/0000-0002-2169-5521

Markus B. Raschke − *Department of Physics, and JILA, University of Colorado at Boulder, Boulder, Colorado 80309, United States*; orcid.org/0000-0003-2822-851X

Michael Lamparski − *Department of Physics, Applied Physics, and Astronomy, Jonsson Rowland Science Center, Troy, New York 12180-3590, United States*

Vincent Meunier − *Department of Physics, Applied Physics, and Astronomy, Jonsson Rowland Science Center, Troy, New York 12180-3590, United States*; orcid.org/0000-0002-7013-179X

Complete contact information is available at: https://pubs.acs.org/10.1021/acs.nanolett.2c00905

Author Contributions

#A.C.G. and V.-H.N. contributed equally to this work.

Notes

The authors declare no competing financial interest.

■ ACKNOWLEDGMENTS

The authors thank Prof Leonardo C. Campos for helpful discussions. This work was supported by CNPq (302775/2018-8), CAPES (RELAII and 88881.198744/2018-01), and FAPEMIG, Brazil. A.C.G. and M.B.R. acknowledge partial support from DoE Award No. DE-SC0008807. V.-H.N. and J.-C.C. acknowledge financial support from the Fédération Wallonie-Bruxelles through the ARC Grants (16/21-077 and 21/26-116), the European Union's Horizon 2020 Research Project, and the Innovation Program Graphene Flagship Core3 (881603), the Flag-Era JTC project "TATTOOS" (R.8010.19), the EOS project "CONNECT" (40007563), and the Belgium F.R.S.-FNRS through the research projects (T.0051.18 and T.029.22). V.M. and M.L acknowledge support from NY State Empire State Development's Division of Science, Technology, and Innovation (NYSTAR). Computational resources have been provided by the CISM supercomputing facilities of UCLouvain and the CÉCI consortium funded by F.R.S.-FNRS of Belgium (2.5020.11).

■ REFERENCES

(1) Pisana, S.; Lazzeri, M.; Casiraghi, C.; Novoselov, K. S.; Geim, A. K.; Ferrari, A. C.; Mauri, F. Breakdown of the adiabatic Born-Oppenheimer approximation in graphene. *Nat. Mater.* **2007**, *6*, 198−201.

(2) Lazzeri, M.; Mauri, F. Nonadiabatic Kohn anomaly in a doped graphene monolayer. *Phys. Rev. Lett.* **2006**, *97*, 266407.

(3) Bonini, N.; Lazzeri, M.; Marzari, N.; Mauri, F. Phonon anharmonicities in graphite and graphene. *Phys. Rev. Lett.* **2007**, *99*, 176802.

(4) Hasdeo, E. H.; Nugraha, A. R.; Dresselhaus, M. S.; Saito, R. Fermi energy dependence of first-and second-order Raman spectra in graphene: Kohn anomaly and quantum interference effect. *Phys. Rev. B* **2016**, *94*, 075104.

(5) Yan, J.; Henriksen, E. A.; Kim, P.; Pinczuk, A. Observation of anomalous phonon softening in bilayer graphene. *Phys. Rev. Lett.* **2008**, *101*, 136804.

(6) Mafra, D. L.; Malard, L. M.; Doorn, S. K.; Htoon, H.; Nilsson, J.; Castro Neto, A. H.; Pimenta, M. A. Observation of the Kohn anomaly near the K point of bilayer graphene. *Phys. Rev. B* **2009**, *80*, 241414.

(7) Das, A.; Chakraborty, B.; Piscanec, S.; Pisana, S.; Sood, A.; Ferrari, A. Phonon renormalization in doped bilayer graphene. *Phys. Rev. B* **2009**, *79*, 155417.

(8) Mafra, D.; Gava, P.; Malard, L.; Borges, R.; Silva, G.; Leon, J.; Plentz, F.; Mauri, F.; Pimenta, M. Characterizing intrinsic charges in top gated bilayer graphene device by Raman spectroscopy. *Carbon* **2012**, *50*, 3435−3439.

(9) Lazzeri, M.; Piscanec, S.; Mauri, F.; Ferrari, A.; Robertson, J. Phonon linewidths and electron-phonon coupling in graphite and nanotubes. *Phys. Rev. B* **2006**, *73*, 155426.

(10) Tsang, J.; Freitag, M.; Perebeinos, V.; Liu, J.; Avouris, P. Doping and phonon renormalization in carbon nanotubes. *Nat. Nanotechnol.* **2007**, *2*, 725−730.

(11) Farhat, H.; Son, H.; Samsonidze, G. G.; Reich, S.; Dresselhaus, M.; Kong, J. Phonon softening in individual metallic carbon nanotubes due to the Kohn anomaly. *Phys. Rev. Lett.* **2007**, *99*, 145506.

(12) Jorio, A.; Dresselhaus, M. S.; Saito, R.; Dresselhaus, G. *Raman Spectroscopy in Graphene Related Systems*; John Wiley & Sons, 2011.

(13) Dresselhaus, M.; Jorio, A.; Saito, R. Characterizing graphene, graphite, and carbon nanotubes by Raman spectroscopy. *Annu. Rev. Condens. Matter Phys.* **2010**, *1*, 89−108.

(14) Allard, A.; Wirtz, L. Graphene on metallic substrates: suppression of the Kohn anomalies in the phonon dispersion. *Nano Lett.* **2010**, *10*, 4335−4340.
(15) Forster, F.; Molina-Sanchez, A.; Engels, S.; Epping, A.; Watanabe, K.; Taniguchi, T.; Wirtz, L.; Stampfer, C. Dielectric screening of the Kohn anomaly of graphene on hexagonal boron nitride. *Phys. Rev. B* **2013**, *88*, 085419.
(16) Wang, X.; Christopher, J. W.; Swan, A. K. 2D Raman band splitting in graphene: Charge screening and lifting of the K-point Kohn anomaly. *Sci. Rep.* **2017**, *7*, 13539.
(17) Nguyen, K. T.; Abdula, D.; Tsai, C.-L.; Shim, M. Temperature and gate voltage dependent Raman spectra of single-layer graphene. *ACS Nano* **2011**, *5*, 5273−5279.
(18) Li, G.; Luican, A.; Lopes dos Santos, J. M. B.; Castro Neto, A. H.; Reina, A.; Kong, J.; Andrei, E. Y. Observation of Van Hove singularities in twisted graphene layers. *Nat. Phys.* **2010**, *6*, 109−113.
(19) Jorio, A.; Cançado, L. G. Raman spectroscopy of twisted bilayer graphene. *Solid State Commun.* **2013**, *175*, 3−12.
(20) Cao, Y.; Fatemi, V.; Fang, S.; Watanabe, K.; Taniguchi, T.; Kaxiras, E.; Jarillo-Herrero, P. Unconventional superconductivity in magic-angle graphene superlattices. *Nature* **2018**, *556*, 43−50.
(21) Yoo, H.; Engelke, R.; Carr, S.; Fang, S.; Zhang, K.; Cazeaux, P.; Sung, S. H.; Hovden, R.; Tsen, A. W.; Taniguchi, T.; et al. Atomic and electronic reconstruction at the van der Waals interface in twisted bilayer graphene. *Nat. Mater.* **2019**, *18*, 448−453.
(22) Gargiulo, F.; Yazyev, O. V. Structural and electronic transformation in low-angle twisted bilayer graphene. *2D Materials* **2018**, *5*, 015019.
(23) Gadelha, A. C.; Ohlberg, D. A.; Rabelo, C.; Neto, E. G.; Vasconcelos, T. L.; Campos, J. L.; Lemos, J. S.; Ornelas, V.; Miranda, D.; Nadas, R.; et al. Localization of lattice dynamics in low-angle twisted bilayer graphene. *Nature* **2021**, *590*, 405−409.
(24) Lee, J. E.; Ahn, G.; Shim, J.; Lee, Y. S.; Ryu, S. Optical separation of mechanical strain from charge doping in graphene. *Nat. Commun.* **2012**, *3*, 1024.
(25) Cocemasov, A. I.; Nika, D. L.; Balandin, A. A. Phonons in twisted bilayer graphene. *Phys. Rev. B* **2013**, *88*, 035428.
(26) Mueller, N. S.; Heeg, S.; Alvarez, M. P.; Kusch, P.; Wasserroth, S.; Clark, N.; Schedin, F.; Parthenios, J.; Papagelis, K.; Galiotis, C.; et al. Evaluating arbitrary strain configurations and doping in graphene with Raman spectroscopy. *2D Materials* **2018**, *5*, 015016.
(27) Lamparski, M.; Van Troeye, B.; Meunier, V. Soliton signature in the phonon spectrum of twisted bilayer graphene. *2D Materials* **2020**, *7*, 025050.
(28) Gadelha, A. C.; Vasconcelos, T. L.; Cançado, L. G.; Jorio, A. Nano-optical Imaging of In-Plane Homojunctions in Graphene and MoS2 van der Waals Heterostructures on Talc and SiO2. *J. Phys. Chem. Lett.* **2021**, *12*, 7625−7631.
(29) Einenkel, M.; Efetov, K. B. Possibility of superconductivity due to electron-phonon interaction in graphene. *Phys. Rev. B* **2011**, *84*, 214508.
(30) Profeta, G.; Calandra, M.; Mauri, F. Phonon-mediated superconductivity in graphene by lithium deposition. *Nat. Phys.* **2012**, *8*, 131−134.
(31) Wu, F.; MacDonald, A.; Martin, I. Theory of phonon-mediated superconductivity in twisted bilayer graphene. *Phys. Rev. Lett.* **2018**, *121*, 257001.
(32) Choi, Y. W.; Choi, H. J. Strong electron-phonon coupling, electron-hole asymmetry, and nonadiabaticity in magic-angle twisted bilayer graphene. *Phys. Rev. B* **2018**, *98*, 241412.
(33) Lian, B.; Wang, Z.; Bernevig, B. A. Twisted bilayer graphene: a phonon-driven superconductor. *Phys. Rev. Lett.* **2019**, *122*, 257002.
(34) Wu, F.; Hwang, E.; Das Sarma, S. Phonon-induced giant linear-in-T resistivity in magic angle twisted bilayer graphene: Ordinary strangeness and exotic superconductivity. *Phys. Rev. B* **2019**, *99*, 165112.
(35) Lewandowski, C.; Chowdhury, D.; Ruhman, J. Pairing in magic-angle twisted bilayer graphene: role of phonon and plasmon umklapp. *Phys. Rev. B* **2021**, *103*, 235401.
(36) Choi, Y. W.; Choi, H. J. Dichotomy of Electron-Phonon Coupling in Graphene Moiré Flat Bands. *Phys. Rev. Lett.* **2021**, *127*, 167001.
(37) Gadelha, A. C.; Ohlberg, D. A.; Santana, F. C.; Eliel, G. S.; Lemos, J. S.; Ornelas, V.; Miranda, D.; Nadas, R. B.; Watanabe, K.; Taniguchi, T.; et al. Twisted bilayer graphene: a versatile fabrication method and the detection of variable nanometric strain caused by twist-angle disorder. *ACS Applied Nano Materials* **2021**, *4*, 1858−1866.
(38) Ohlberg, D. A.; Tami, D.; Gadelha, A. C.; Neto, E. G.; Santana, F. C.; Miranda, D.; Avelino, W.; Watanabe, K.; Taniguchi, T.; Campos, L. C.; et al. The limits of near field immersion microwave microscopy evaluated by imaging bilayer graphene moiré patterns. *Nat. Commun.* **2021**, *12*, 2980.
(39) Taychatanapat, T.; Jarillo-Herrero, P. Electronic transport in dual-gated bilayer graphene at large displacement fields. *Phys. Rev. Lett.* **2010**, *105*, 166601.
(40) Barbosa, T. C; Gadelha, A. C; Ohlberg, D. A A; Watanabe, K.; Taniguchi, T.; Medeiros-Ribeiro, G.; Jorio, A.; Campos, L. C Raman spectra of twisted bilayer graphene close to the magic angle. *2D Materials* **2022**, *9*, 025007.
(41) Park, C.-H.; Giustino, F.; Cohen, M. L.; Louie, S. G. Electron-Phonon Interactions in Graphene, Bilayer Graphene, and Graphite. *Nano Lett.* **2008**, *8*, 4229−4233.
(42) Hung Nguyen, V.; Paszko, D.; Lamparski, M.; Van Troeye, B.; Meunier, V.; Charlier, J.-C. Electronic localization in small-angle twisted bilayer graphene. *2D Materials* **2021**, *8*, 035046.
(43) Kerelsky, A.; McGilly, L. J.; Kennes, D. M.; Xian, L.; Yankowitz, M.; Chen, S.; Watanabe, K.; Taniguchi, T.; Hone, J.; Dean, C.; et al. Maximized electron interactions at the magic angle in twisted bilayer graphene. *Nature* **2019**, *572*, 95.
(44) Cea, T.; Walet, N. R.; Guinea, F. Electronic band structure and pinning of Fermi energy to Van Hove singularities in twisted bilayer graphene: A self-consistent approach. *Phys. Rev. B* **2019**, *100*, 205113.
(45) Rademaker, L.; Abanin, D. A.; Mellado, P. Charge smoothening and band flattening due to Hartree corrections in twisted bilayer graphene. *Phys. Rev. B* **2019**, *100*, 205114.
(46) Cea, T.; Guinea, F. Band structure and insulating states driven by Coulomb interaction in twisted bilayer graphene. *Phys. Rev. B* **2020**, *102*, 045107.
(47) Goodwin, Z. A. H.; Vitale, V.; Liang, X.; Mostofi, A. A.; Lischner, J. Hartree theory calculations of quasiparticle properties in twisted bilayer graphene. *Electronic Structure* **2020**, *2*, 034001.
(48) Lewandowski, C.; Nadj-Perge, S.; Chowdhury, D. Does filling-dependent band renormalization aid pairing in twisted bilayer graphene? *npj Quantum Mater.* **2021**, *6*, 82.
(49) Cea, T.; Guinea, F. Coulomb interaction, phonons, and superconductivity in twisted bilayer graphene. *Proc. Natl. Acad. Sci. U. S. A.* **2021**, *118* (32), e2107874118.
(50) Gunst, T.; Markussen, T.; Stokbro, K.; Brandbyge, M. First-principles method for electron-phonon coupling and electron mobility: Applications to two-dimensional materials. *Phys. Rev. B* **2016**, *93*, 035414.
(51) Kim, S.; Jo, I.; Dillen, D. C.; Ferrer, D. A.; Fallahazad, B.; Yao, Z.; Banerjee, S. K.; Tutuc, E. Direct Measurement of the Fermi Energy in Graphene Using a Double-Layer Heterostructure. *Phys. Rev. Lett.* **2012**, *108*, 116404.

https://doi.org/10.1021/acs.nanolett.2c00905
Nano Lett. 2022, 22, 6069−6074